

# Integrating Physics-Based Wireless Propagation Models and Network Protocol Design for Train Communication Systems

Neeraj Sood, *Student Member, IEEE*, Sami Baroudi, *Member, IEEE*, Xingqi Zhang, *Student Member, IEEE*, Jörg Liebeherr, *Fellow, IEEE* and Costas D. Sarris, *Senior Member, IEEE*

**Abstract**—Physics-based wireless propagation modeling and network protocol design have evolved over decades as orthogonal areas in communication systems research. This fragmented approach does not exploit available efficiencies when planning and deploying communication systems. In an attempt to integrate the two areas we harness the understanding of the underlying physics of electromagnetic propagation to enhance the robustness of network protocol design by deriving physics-based network-level performance metrics. We use ray-tracing and parabolic equation models of 2.4 GHz propagation along tunnel and open-air sections of London Underground to evaluate the performance of a communications-based train control (CBTC) system. For comparison, we consider existing path loss models for tunnel environments and investigate whether they can provide sufficient accuracy to be used for network protocol design. We show that physics-based models lead to reliable predictions at the network level, similar in fidelity to using measured data and unlike using simplified channel models of the path loss exponent type.

**Index Terms**—Radio propagation, channel models, ray tracing, finite difference methods, network protocol design.

## I. INTRODUCTION

The continuing proliferation of wireless train control systems has intertwined the development of rail signaling with advances in information and communication technologies. This connection has led to the evolution of Communications-Based Train Control (CBTC), which is aimed at replacing conventional rail signaling with train control enabled by wireless communication between trains and access points (APs) deployed along the track [1]–[3].

As is very common with other communication networks, the design of CBTC systems has relied on a rather fragmented approach. First, the deployment of access points relies on the characterization of the propagation channel, which is pursued by measurements, modeling or a combination of the two. This channel characterization problem is based on knowledge of the antenna radiation properties, as well as the geometric and material specification of the environment (Fig. 1(a)). Relevant quantities of interest are the electromagnetic field components and ultimately the received signal strength (RSS). The final positions of the access points are determined by ensuring that RSS levels throughout the channel meet certain criteria, for example, surpassing a minimum threshold value everywhere. With the network infrastructure in place, communication protocols are subsequently established (Fig. 1(b)). While a significant volume of work has been carried out in these two areas independently, their integration can pave the way for far

better, more secure and more reliable rail signaling systems. Network protocol design can benefit by harnessing a deeper understanding of the underlying physics of electromagnetic propagation in guideways.

Radio propagation in tunnels can be modeled using physics-based methods or path loss models calibrated by measurements. Physics-based methods consist of analytical approaches such as waveguide theory and simulation techniques such as vector parabolic equation (VPE) and ray tracing [4]. Waveguide theory provides efficient and accurate results for canonical geometries [5]–[9] by making the analogy between wave propagation in tunnels with overmoded waveguides, however, it is too restrictive for complex tunnel environments. In [10], it was shown that the mapping of a general arched tunnel to a waveguide model is not unique and depends on the position of the transmitter and receiver. Hence, it is a surrogate model of particular transmitter-receiver positions within the tunnel, rather than a global model. On the other hand, VPE has found a prolific area of application in long guiding structures combining computational efficiency with numerical accuracy [11], [12]. Since VPE is derived from the full-wave Helmholtz equation, the effects of reflection, diffraction, and radiation can be taken into account. More recently, improved VPE techniques have been introduced to enable propagation modeling in curved tunnels with various cross section geometries [13]–[16]. Similarly, ray tracing based on geometrical optics and the uniform theory of diffraction can be utilized to characterize tunnels with arbitrary geometries [17], [18], although it can be quite computationally intensive depending on the underlying geometrical detail. Additionally, applying these methods to arched or curved tunnels leads to inaccuracies, specifically, a significant overprediction of power as the number of facets approximating the tunnel cross section increases [19]. Alternatively, path loss models are parametric models for which the relevant parameters are extracted by fitting the models to measured data [20]–[27]. These models provide helpful insights into the propagation characteristics of the studied channels; but they are not expected to provide an accurate RSS estimate on a point-by-point basis, within the channel.

In this paper, we investigate if and to what degree physics-based propagation models can be used to improve network planning for train communication systems in tunnels, with the potential to influence other safety critical applications as well. In this manner, we overcome the virtual separation of

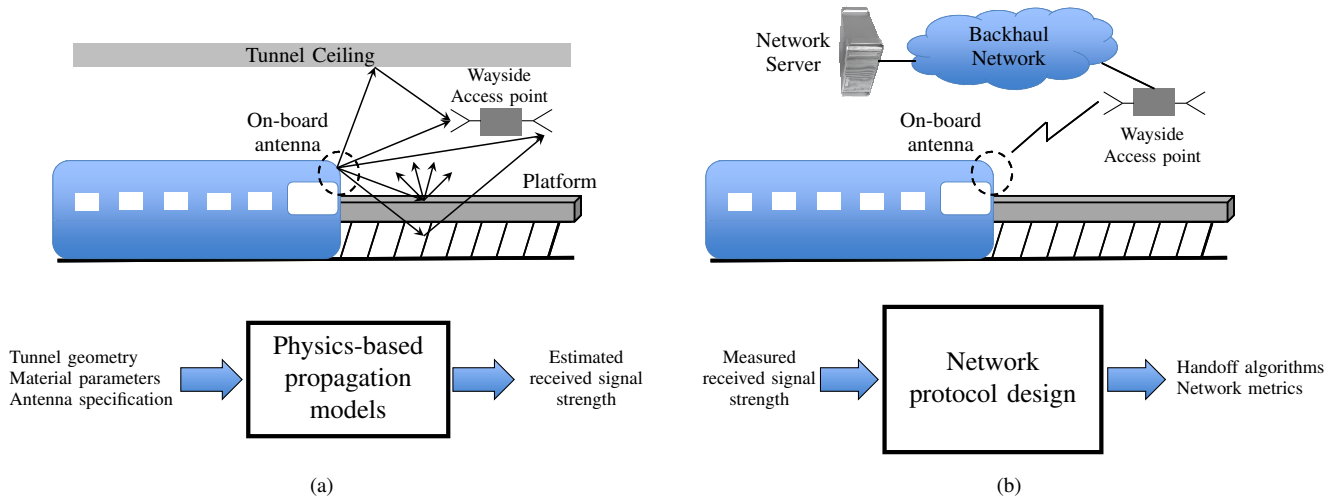


Fig. 1. Approaches for CBTC analysis and design from (a) an electromagnetics perspective, and (b) a network protocol perspective.

network design along disciplinary boundaries by bridging the gap between the output of physics-based propagation models and the input of network protocol design (see Fig. 1). To accomplish this, we use RSS measurements at 2.4 GHz carried out in a complex tunnel environment in London, UK, as a benchmark against which the fidelity of estimated RSS models is compared. Ray tracing and VPE based methods are employed to generate the estimated RSS. These physics-based propagation models require a geometrical description of the modeled environment which is generated using three-dimensional data points captured via a laser survey. For comparison, we consider path loss models to estimate RSS in tunnels, and discuss their limitations. Subsequently, measured, simulated and estimated (from path loss models) RSS values are integrated in a network-level simulation to determine the *handoff map* of the network. The handoff map is related to the fact that as the train moves along the track, the RSS of the associated AP changes as a function of the current train location. A train en route changes the association by selecting a new AP. The process of changing the association from one AP to another is called handoff. A handoff algorithm describes when and to which AP the train should perform the handoff [28]. The record of handoffs, (the handoff map) provides knowledge of the number and location of the handoffs.

The rest of the paper is organized as follows. In Section II we describe the tunnel geometry and the measurement setup. These measurements are carried out in a complex tunnel environment in London, UK. In Section III we present the physics-based simulation methods, VPE and ray tracing, to estimate RSS along the aforementioned tunnel subsequently comparing predicted and measured RSS. In Section IV we discuss existing path loss models used to model propagation characteristics in tunnel environments and their limitations. In Section V we employ the propagation models described in earlier sections to evaluate performance metrics for handoff algorithms in a CBTC system and compare their accuracy. We conclude the paper in Section VI.

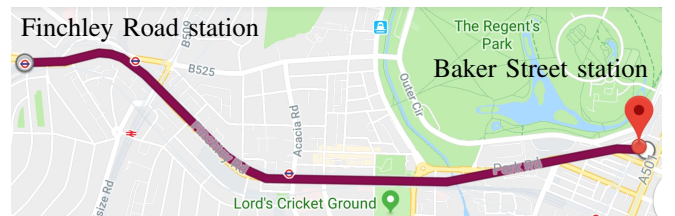


Fig. 2. Map highlighting the track from Baker Street station to Finchley Road station.

## II. MEASUREMENT CAMPAIGN

This section describes a measurement campaign conducted by Thales Canada and UK to determine the propagation characteristics of a tunnel environment and map its geometrical detail. The measured RSS values will be used in later sections to determine the handoff map of a CBTC system deployed in this environment, prompting comparisons with such maps derived by using physics-based propagation and simplified path loss models. In the following subsections, we discuss the tunnel geometry and measurement setup pertinent to the measurement campaign.

### A. Tunnel Geometry

The studied geometry is a 3.5 km guideway consisting of tunnel and open-air sections covering the region from Finchley Road station to Baker Street station which is a part of the London Underground network in London, UK, as shown in Fig. 2. The tunnel consists of sections with arched and rectangular cross sections; a few of them also transition into open-air regions. The tunnel is predominantly either single-track (narrow, 4.4 m wide) or dual-track (wide, 7.4 m wide). The exact geometry of the tunnel is mapped using a laser scanner resulting in a three dimensional representation, referred to as a *point cloud*. The point cloud consists of cross-sectional cuts along the axis of the tunnel, referred to as *slices*, which are obtained approximately every 0.5 m. The points representing each slice are all described using a common coordinate system.

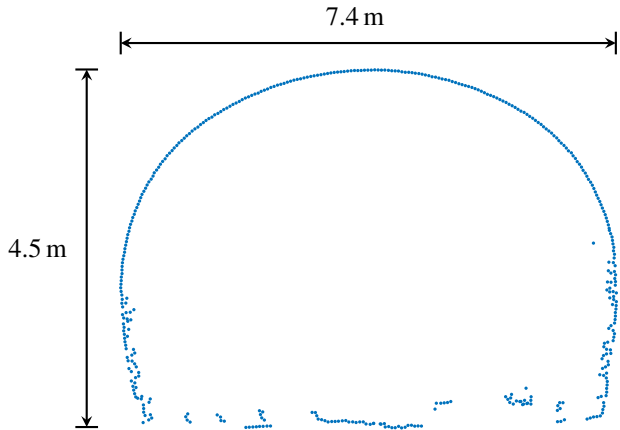


Fig. 3. Arched dual-track cross section.

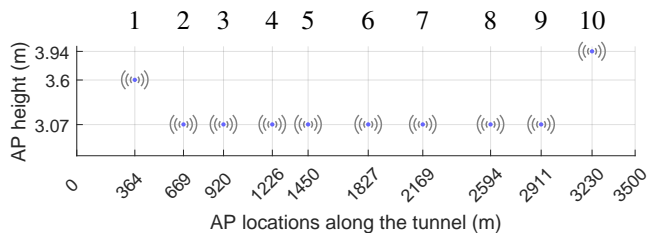


Fig. 4. AP heights and locations along the tunnel.

TABLE I  
CROSS SECTION INFORMATION FOR ALL APs.

AP index	cross section type	Width
1	Rectangular	Single
2	Arched	Dual
3	Arched	Single
4	Arched	Single
5	Arched, Open-Air	Dual
6	Arched	Single
7	Arched	Single
8	Rectangular, Open-Air	Dual
9	Arched	Single
10	Rectangular	Dual

Hence, this data set not only captures the cross-sectional but also the elevation and curvature information along the tunnel. The point cloud data are processed to generate the input geometry for the physics-based simulation methods presented in the next section. Fig. 3 shows the point cloud data corresponding to an arched dual-track tunnel section.

### B. Measurement Setup

The measured system consists of 10 APs distributed throughout the entire tunnel as shown in Fig. 4. The height of each AP relative to the ground is indicated on the  $y$ -axis. Table I lists the cross section information of the region covered by each AP. Each AP in the system is equipped with a 14 dBi vertically polarized Yagi antenna in transmit mode. The

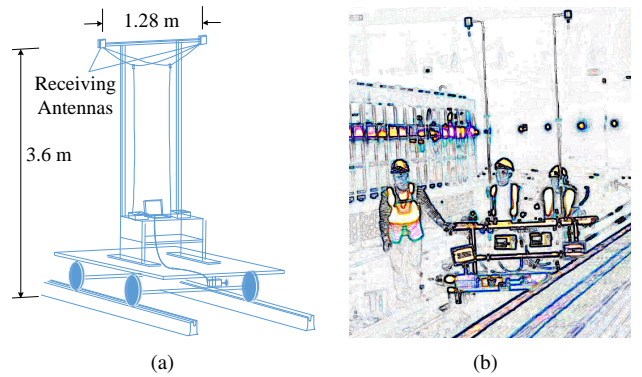


Fig. 5. (a) Schematic and (b) photograph of the trolley with the receiving antennas mounted. Source: Thales Canada

operating frequency is 2.44 GHz and the effective isotropic radiated power (EIRP) is 20 dBm.

The receiving antennas, emulating the antennas on the train and operating in a continuous wave (CW) mode, are mounted on a trolley that is driven down the tracks of the London Underground line from Baker Street station to Finchley Road station. Each receiver is connected to a low noise amplifier, which is in turn connected to a spectrum analyzer. The receivers are mounted at a height of 3.6 m and are horizontally separated by 1.28 m. The representative received signal strength at each sampled location is the maximum of the power captured by the two receivers. **The whole trolley setup has been designed to minimize the influence of the trolley equipment and its operators on the antenna pattern. As shown in Figs. 5(a), 5(b), the trolley and the operators are in the far field of the antennas and away from their broadside direction, where their directivity reaches its maximum of 9 dBi. Therefore, we have not included the trolley and its operators in our simulations.**

The sampling interval between two consecutive measurements is 1 m. Since large scale fading is of importance for network planning, small-scale fading is filtered from the received signal by averaging the power using a moving window of 40 wavelengths [29].

### III. PHYSICS-BASED SIMULATION METHODS

In this section, we discuss the application of ray tracing and VPE to model the propagation characteristics of the London underground guideway previously described. Section III-A introduces the basic ray tracing method, as well as modifications that have been made to increase its accuracy for complex tunnel environments. Section III-B presents the corresponding treatment for the VPE method. Subsequently, these two methods are briefly compared in Section III-C. Section III-D presents a comparison of the RSS estimated by ray tracing and VPE with the measured RSS as the benchmark.

#### A. Ray Tracing

We use the three-dimensional image-based ray tracing solver originally presented in [30] and subsequently improved in [31]. Ray tracing algorithms based on the method of images

provide a systematic way of generating the ray path trajectory from the transmitter (Tx) to the receiver (Rx). The method uses image theory in order to generate higher order image sources that correspond to ray paths that have undergone a specified number of reflections. These algorithms can only be applied to an environment that is described using planar facets.

1) *Fundamentals of Ray Tracing*: The ray tracing method can be decomposed into two main steps, namely, the generation of ray paths and calculation of the corresponding electromagnetic fields associated with each path.

Ray paths can be systematically calculated by constructing an image tree, which is a data structure that stores image sources corresponding to all potential ray paths that could exist in a given environment between a transmitter and a receiver [32]. After computing the geometry, of all the considered ray paths, the total electric field at the Rx,  $\mathbf{E}$ , is calculated as the superposition of the electric fields associated with paths,  $\mathbf{E}_i$ , using

$$\mathbf{E} = \sum_{i=1}^N \mathbf{E}_i \quad (1)$$

where  $N$  is the total number of ray paths considered. The electric field associated with the direct ray is computed as

$$\mathbf{E}_{\text{dir}} = \sqrt{\frac{\eta P_r G}{2\pi}} \mathbf{U}_0(\theta, \phi) \frac{e^{-jk_0 r}}{r} \quad (2)$$

where  $\eta$  is the free-space impedance,  $P_r$  is the transmitted power,  $G$  is the gain of the transmitter,  $k_0$  is the free-space wave number which given by  $2\pi/\lambda$ , where  $\lambda$  is the wavelength,  $\mathbf{U}_0(\theta, \phi)$  is the normalized radiation pattern of the Tx, and  $(r, \theta, \phi)$  is the observation point in the spherical co-ordinate system with the Tx location as the origin. The electric field associated with each indirect ray is computed by decomposing the incident electric field into the parallel (TM) and perpendicular (TE) components with respect to the plane of incidence and then applying the appropriate Fresnel reflection coefficient. The open-circuited voltage,  $V_{\text{oc}}$  across the receiving antenna is calculated from the electric fields,  $\mathbf{E}_i$ , using its vector effective length [33],  $\mathbf{l}_{\text{eff}}$ , as

$$V_{\text{oc}} = \sum_{i=1}^N \mathbf{E}_i \cdot \mathbf{l}_{\text{eff}}(\theta_i, \phi_i) \quad (3)$$

Subsequently, the received power,  $P_R$  under matched conditions is obtained as

$$P_R = \frac{|V_{\text{oc}}|^2}{8R_r} \quad (4)$$

where  $R_r$  is the radiation resistance of the receiving antenna.

2) *Ray Tracing Simulation Setup*: A facetized model of the environment forms the input of the ray tracing method as it is necessary to compute the ray paths. This geometry is extracted from the point cloud data, which is partitioned into slices corresponding to cross-sectional cuts along the axis of the tunnel. The slices that should be included in the input model are determined based on two criteria – cross-section type and track direction. A new slice is added to the model whenever the tunnel cross-section type changes (e.g. single-track to dual-track or rectangular to arched) or when the angle between

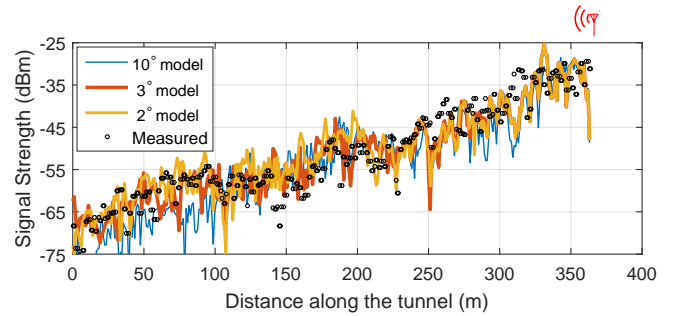


Fig. 6. Received signal strength along the tunnel for AP-1 for varying level of tunnel geometry.

the local tangent at a candidate location and the reference location surpasses a threshold value. Therefore, by selecting a threshold value for this angle, locations of the significant slices can be determined. Fig. 6 shows the comparison of the received signal strength along the tunnel region covered by AP-1 for models generated using a threshold of  $10^\circ$ ,  $3^\circ$ , and  $2^\circ$ . The location of the AP is indicated with a red antenna symbol. The results show that adding a slice corresponding to a  $2^\circ$  threshold is adequate. After selecting these significant slices, the cross section of each slice needs to be approximated using piecewise linear segments. The choice of the number of segments used for this approximation is very critical. If the number of segments is too small, then the geometry of the ray paths is not sufficiently accurate. On the other hand, if the number of segments is too large, the resulting electric field values produce a significant overprediction in the received power [19]. The results shown in this paper are generated with the input models employing seven segments to approximate each slice of the arched cross sections [31]. Moreover, all facets approximating the tunnel are assumed to be concrete and, therefore, have a relative permittivity,  $\epsilon_r$ , of 5 and a conductivity,  $\sigma$ , of 0.001 S/m. Additionally, each considered ray path can have a maximum of six reflections, which on average results in the superposition of around 80 ray paths in total to compute the electric field at any sampled location.

The large number of reflections and ray paths needed to extract convergent ray-tracing results is not surprising, considering that some of the earliest models of radiowave propagation in tunnels were based on waveguide mode theory [5]–[7]. Once we intuitively understand radiowave propagation in tunnels in terms of guided modes, we also have to expect that these modes will be mapped to a significant number of reflected paths, unlike open environments where only few reflections may be adequate.

## B. Vector Parabolic Equation Method

The parabolic equation is an approximation of the Helmholtz wave equation, which assumes that fields have slow variations along the propagation direction. This assumption leads to the reduction of the elliptical Helmholtz wave equation to a parabolic equation with respect to the transverse components of the fields [34]. This greatly reduces the computational cost of solving large scale propagation problems and

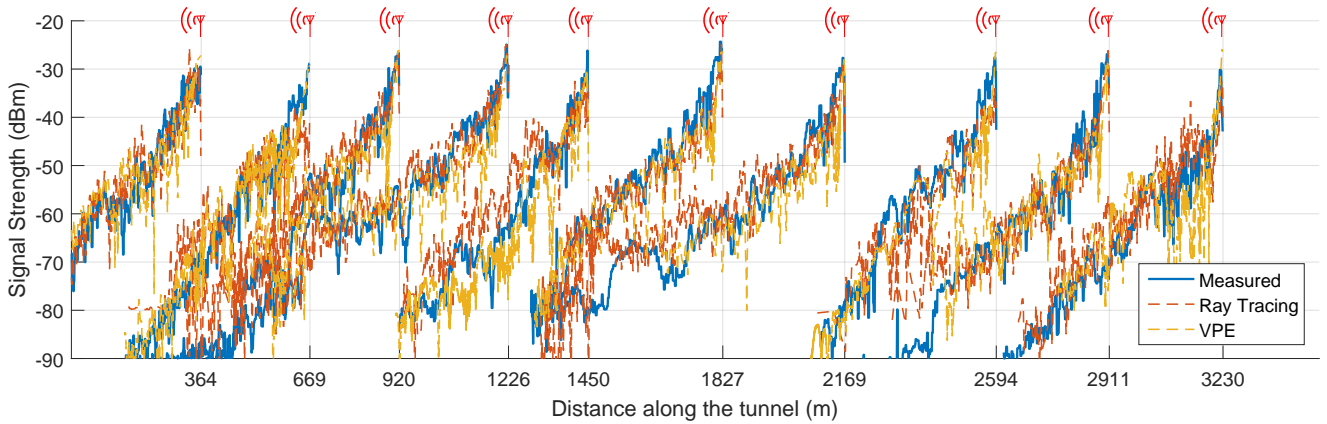


Fig. 7. Comparison of signal strength (in dBm) along the tunnel as received by the receiver antenna on the train, from each of the 10 APs for the CBTC system, along the Baker-Finchley line (see Fig. 2).

allows for the application of numerical methods for parabolic equations, including unconditionally stable solvers. The three dimensional VPE solver presented in [14], [16] is used in this paper.

1) *Fundamentals of VPE*: Assuming propagation predominantly along the  $z$ -axis, the standard parabolic equation can be expressed as:

$$\frac{\partial u}{\partial z} = \frac{1}{2jk_0} \left( \frac{\partial^2}{\partial x^2} + \frac{\partial^2}{\partial y^2} \right) u \quad (5)$$

where  $u$  is the reduced plane wave solution under the paraxial approximation [34] and  $k_0$  is the free-space wave number. A vectorial form of (5), referred to as the vector parabolic equation, is used to determine all field components at one step and address the coupling effects [34].

A commonly used finite-difference scheme solving (5) is the Alternating-Direction-Implicit (ADI) method. The ADI method is unconditionally stable and second-order accurate in all spatial variables  $x$ ,  $y$ , and  $z$ . The ADI method is very efficient because multi-dimensional fields are updated along one dimension at a time [12]. A comprehensive error analysis and comparative study of numerical methods for the parabolic equation applied to radio-wave propagation modeling is presented in [35].

2) *VPE Simulation Setup*: Similar to ray tracing, the input geometry for VPE is extracted from the point cloud data. Successive slices that have more than 10% variations in the cross section area are included in the construction of the input model. After selecting those significant slices, instead of using piece-wise linear segments, a smooth polynomial curve is used to fit each cross section profile.

### C. Ray Tracing vs. Vector Parabolic Equation

VPE is computationally efficient as it is based on a paraxial approximation of the wave equation [15], [34]. Therefore, it is well suited for tunnel environments [12]. On the other hand, image-based ray tracing is based on a facetized approximation of the geometry of the tunnel, which has a significant impact on the accuracy of the solution [36]. VPE does not suffer from this problem, as it applies boundary conditions on a curve

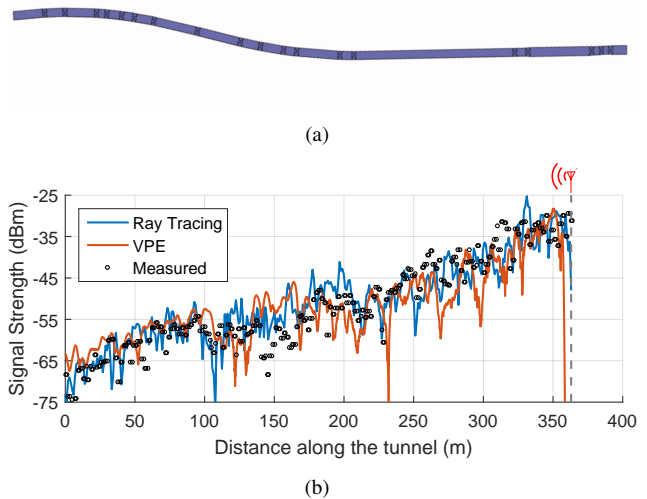


Fig. 8. (a) Facetized input geometry for the tunnel section covered by AP-1. (b) Comparison of received signal strength along the tunnel for AP-1.

that exactly follows the tunnel cross-section. Ray tracing is more capable at handling arbitrary channel geometries [37]. Therefore, both methods have their benefits and drawbacks. The accuracy of these physics-based models will be discussed in the next subsection and the extent to which it effects the computation of network level performance metrics will be studied in Section V.

### D. Simulation Results

The ray tracing and VPE solvers described in Section III-A and Section III-B are used to estimate the RSS along the tunnel for all 10 APs described in Section II-A. The estimated RSS is compared with measurements to validate both solvers. Fig. 7 shows the RSS for all 10 APs corresponding to ray tracing, VPE, and measurements. Additionally, the same comparison of RSS for AP-1 and AP-3 and their corresponding input geometry is shown in Figs. 8 and 9, where the red antenna symbol indicates the AP location. As seen in the figures,

TABLE II  
AMD BETWEEN THE MEASURED AND SIMULATED RSS FOR ALL APs.

AP	1	2	3	4	5	6	7	8	9	10
Ray Tracing	4.01	6.09	6.13	5.2	6.3	3.78	5.25	5.5	5.55	5.39
VPE	4.68	4.64	4.5	5.14	4.92	3.98	4.41	5.02	4.62	6.02

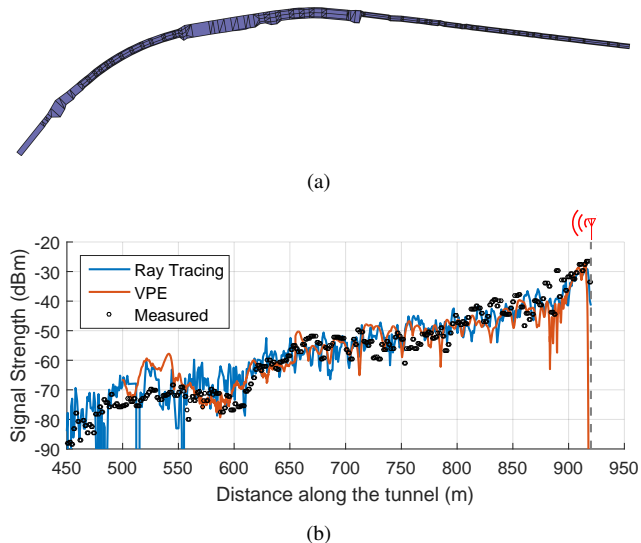


Fig. 9. (a) Facetized input geometry for the tunnel section covered by AP-3. (b) Comparison of received signal strength along the tunnel for AP-3.

both ray tracing and VPE achieve good overall agreement with the measurements with predominantly minor local deviations. In order to numerically quantify the deviation in ray tracing and VPE, the absolute mean deviation (AMD) [38] in the RSS between each simulated model and measurement data is evaluated by

$$\Delta = \frac{1}{p} \sum_{i=1}^p |P_{R,i}^{\text{meas}} - P_{R,i}^{\text{sim}}| \quad (6)$$

where  $\Delta$  is the AMD,  $p$  is the total number of receiver locations sampled,  $P_{R,i}^{\text{meas}}$  is the measured RSS of the  $i$ -th sampled point, and  $P_{R,i}^{\text{sim}}$  is the estimated RSS at the same point using ray tracing and VPE. The resulting AMD values for all APs are listed in Table II.

The AMD values are correlated with the geometrical complications that exist in the regions being modeled. In particular, the region covered by AP-2 and AP-3 contains multiple complex transitions, especially near the location of the APs. Further, the region covered by AP-5 and AP-8 contains significant length of open-air sections. Additionally, it should be noted that in order to build the input models for the simulations, relevant geometrical detail is included as discussed in Section II-A. Finer details which are laborious to measure such as wires running along the tunnel are intentionally left out. This finite granularity introduces minor local deviations, however, it does not compromise the ability of ray tracing and VPE to accurately extract the large-scale path loss features of the channel, as shown in Figs. 7, 8, and 9. In Section V,

the impact of these deviations in ray tracing and VPE on the accuracy of the handoff map for this system will be explored. This is done with the goal of assessing how the observed differences in measured and simulated data in terms of path loss influence network-level simulations.

#### IV. PATH LOSS MODELS FOR PROPAGATION IN TUNNELS

In this section, we review recent path loss models for tunnel environments, as they can be convenient alternatives to propagation models such as ray-tracing and VPE to extract RSS estimates in a given environment. While ray-tracing and VPE are subject to numerical errors, as well as errors due to uncertainties in the geometric and material specification of the environment [39], path loss models are also subject to two sources of error. First, we show that there are inherent ambiguities in the process of extracting their parameters from measured data. Second, as general purpose, non-site specific models, they cannot fully capture the propagation effects of rich and complex multipath environments, such as those of tunnels. The first point is illustrated in the following, while the second will be further explored in the next section.

##### A. Background

The path loss,  $L_P(d)$ , at a distance  $d$ , is expressed in dB as [29]

$$L_P(d) = \underbrace{L_P(d_0) + 10n \log_{10}(d/d_0)}_{\text{Propagation Loss}} + X_\sigma \quad (7)$$

where  $n$ , referred to as path loss exponent, indicates the slope of the path loss with respect to the separation distance between Tx and Rx,  $d_0$  is the close-in reference distance,  $d$  is the separation distance between the transmitter and the receiver, and  $X_\sigma$  is a zero-mean Gaussian distributed random variable with standard deviation  $\sigma$ .

Table III presents an overview of path loss models for tunnel environments. The table lists propagation characteristics obtained from measurement campaigns in straight [23], [24], [27] and curved [24]–[27] tunnels for frequencies between 465 MHz and 5.7 GHz. In [22], [23], [25]–[27], the authors extract the path loss exponent by fitting the best-fit line to the measured path loss data in a log-scale. In [23], [25], path loss data at small distances from the transmitter are ignored, enabling the extraction of a single path loss exponent for the remaining data. However, the range of path loss data ignored is somewhat arbitrary in the aforementioned papers. Whereas in [27], the authors extract a single path loss exponent by considering the whole range of path loss data between Tx and Rx. Hence, no path loss data is ignored in contrast with the previous approach. In [22], [26], the authors divide the

TABLE III  
 PROPAGATION CHARACTERISTICS IN TUNNELS.

Scenario	Frequency (MHz)	Path loss exponent	Standard deviation of shadowing (dB)
Straight and curved tunnel [22]	2137.6	$N(0.32,0.49)$ near region	3.5 near region
		$N(3.98,0.97)$ far region	5.1 far region
Quasi-straight tunnel [23]	465	9.72	7.15
	820	8.17	4.58
Straight tunnel [24]	2642	1.94	5.47
Straight and curved tunnel [24]	2642	2.19	5.25
Curved tunnel [25]	920	0.94	4.95
	2400	1.81	3.61
	5705	2.2	3.36
Curved tunnel [26]	2400	1.5 near region	–
		5.4 far region	–
Straight and curved tunnel [27]	2400	1.58	5.9
	5000	1.62	4.4

distances between Tx and Rx into near and far regions and extract a separate path loss exponent for each region. This is done to account for the fundamentally different propagation characteristics in the different regions. The division point between the two regions is chosen to be at 100 m [22] and 23 m/76 m [26].

### B. Path loss exponent extraction

To assess the impact of the ambiguity resulting from the approaches for extracting path loss exponent described in the previous subsection, the measured RSS values from London Underground are analyzed. This is accomplished by extracting the path loss exponent as the slope of the line of best-fit to the measured path loss data. Table IV shows the extracted path loss exponents for different locations of the division point for different cross section types corresponding to AP-1 (rectangular, narrow), AP-2 (arched, dual) and AP-6 (arched, single). The first row in Table IV reports the single path loss exponent

 TABLE IV  
 PATH LOSS EXPONENT EXTRACTED FROM MEASUREMENTS FOR DIFFERENT DIVISION POINT LOCATIONS.

Distance of division point from AP (m)	AP-1		AP-2		AP-6	
	$n_0$	$n_1$	$n_0$	$n_1$	$n_0$	$n_1$
10	–	2.80	–	4.14	–	3.59
25	-0.90	3.28	-0.10	4.75	0.21	3.93
50	0.18	3.62	0.17	5.29	1.90	4.47
75	0.88	3.82	0.97	5.71	1.77	4.95
100	1.26	3.98	1.86	6.39	1.86	5.46

for the entire region covered by an AP. In the subsequent rows, the division point is swept in increments of 25 m. Hence two path loss exponents,  $n_0$  (near region) and  $n_1$  (far region), for the resulting regions are presented, as highlighted in Fig. 10.

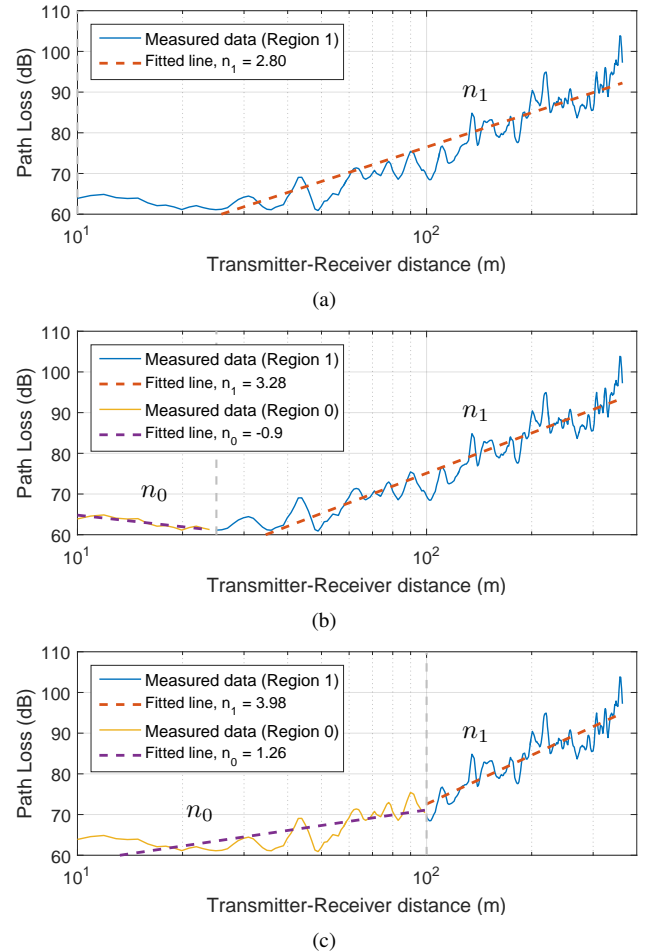


Fig. 10. Path loss (dB) along the tunnel for AP-1 with the best fit (in a least-squares sense) lines for division point located at (a) 10 m (b) 25 m and (c) 100 m from the transmitter.

To illustrate Table IV, Figs. 10(a), 10(b), and 10(c) show the path loss for AP-1 with the corresponding best fit (in a least-squares sense) lines for division points located at distances 0 m, 25 m, and 100 m. The division points are marked on the figures using the dashed vertical lines. The path loss values are evaluated using the link budget equation [40].

As shown in the first row of Table IV and Fig. 10(a), the single path loss exponent does not sufficiently capture the propagation characteristics. This is apparent from the larger AMD between the measured data and the best-fit line in Fig. 10(a) compared to Figs. 10(b) and 10(c). Hence, dividing the studied region into multiple parts understandably yields a more accurate representation. As an example, one division point is introduced at different locations and the corresponding path loss exponents are presented in the remaining rows of Table IV. It can be noticed that the choice of location and number of division points significantly influence the path loss exponents. Thus, apart from the variability introduced in these models due to their non-site specific nature, there is an additional inherent uncertainty due to the choice of the division point. In the next section, we will establish the effect of these errors on the performance metrics related to network planning. This will be done by generating the RSS values from ray tracing, VPE and path loss models, which will in turn be used to generate network-level performance metrics.

## V. FROM PROPAGATION MODELS TO NETWORK-LEVEL SIMULATIONS

In this section, we use a handoff algorithm in a CBTC system to gain insights into the impact of the error in estimating the RSS on network-level performance metrics. This is accomplished by utilizing the RSS values estimated using ray tracing, VPE, path loss models, and measured data in a network operation scenario of a CBTC system.

In a CBTC system, trains communicate with a central control station through APs deployed along the track. As the train moves along the track, the RSS of the associated AP changes as a function of the current train location,  $\mathcal{L}_{\text{train}}$ . Hence, a handoff map, which provides knowledge of the number and location of the handoffs, is chosen as the network-level performance metric.

### A. Handoff Algorithm

We consider an RSS-based handoff algorithm as described in [41] to evaluate the impact of the errors in estimating the RSS on the network-level performance. The method is outlined in the flowchart shown in Fig. 11. At the starting location, the train measures the RSS from all  $m$  APs deployed along the track. It then associates to the AP with the highest RSS. The index corresponding to this AP is denoted as  $j$ . Then  $\mathcal{L}_{\text{train}}$  is incremented by  $\Delta\mathcal{L}$ , which is the distance between two consecutively sampled locations. At each location, the RSS of the associated AP,  $P_R^j$ , is compared to a predefined threshold,  $P_{\text{th}}$ . As long as  $P_R^j$  is greater, the current association is maintained. If  $P_R^j$  falls below  $P_{\text{th}}$ , the train compares the RSS from the other APs,  $\{P_R^i\}$ ,  $i \in \{1, 2, \dots, m\}$ ,  $i \neq j$ , to  $P_R^j$ . If no AP is found with a better RSS, the train retains

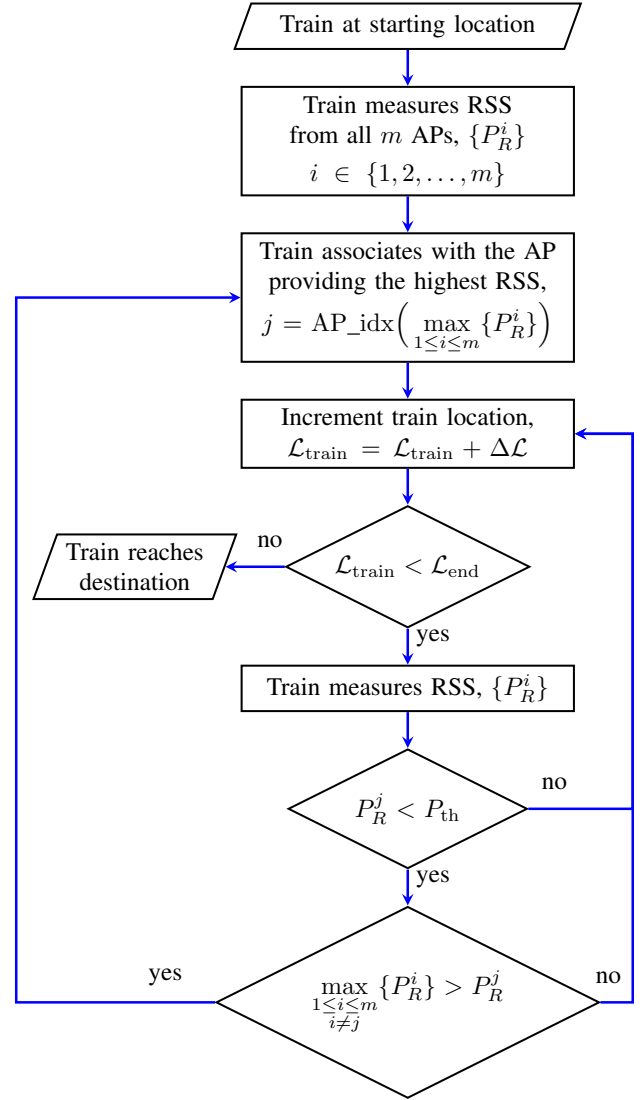


Fig. 11. Flowchart for the RSS-based handoff method.

the current association, otherwise a handoff is initiated to the AP with the best available RSS at  $\mathcal{L}_{\text{train}}$ . This procedure is repeatedly carried out until the train reaches its destination,  $\mathcal{L}_{\text{end}}$ .

### B. Handoff Results

With the handoff algorithm above we can generate handoff maps corresponding to RSS from ray tracing, VPE, path loss models and measured data. These handoff maps are used to determine the correlation between the quality of the various RSS results on network planning. The studied CBTC system deploys 10 APs along the track which is around 3.5 km long as shown in Fig. 4. The coverage threshold,  $P_{\text{th}}$  is chosen to be -70 dBm and the receiver sensitivity is assumed to be -84 dBm [42]. An AP is undetectable if the RSS falls below the receiver sensitivity.

From the list of path loss models in Table III, we select a subset, [25]–[27], where the operating frequency is 2.4 GHz and the measured environment is similar to the one studied

TABLE V  
HANDOFF LOCATIONS AND ASSOCIATED APs CORRESPONDING TO MEASURED DATA AND SIMULATED, AND EMPIRICAL MODELS.

	Associated AP ( $j$ )	1	2	3	4	5	6	7	8	9	10	# Handoffs
	Measured data	0	722	957	1231	–	1807	2267	2444	2936	3292	8
Simulated	Ray tracing	0	620	996	1232	–	1779	2198	2647	2806	3181	8
	VPE	0	725	894	1245	–	1801	2275	2667	2707	3214	8
Empirical	Guan [25]	0	–	1037	–	1473	–	2106	–	2999	–	4
	Liu [26]	0	–	859	–	1413	1940	2306	–	2780	–	5
	Li [27]	0	607	892	1099	1408	1674	2022	2449	2809	3135	9

in this paper. RSS values are then generated for each AP using the path loss model from (7), where the path loss exponent and standard deviation of shadowing are based on the measurement campaigns described in the corresponding papers. RSS values are calculated at the same locations as the measurement campaign described in Section II.

The handoff map derived using the measured RSS forms the benchmark against which the other models are compared. The handoff maps corresponding to ray tracing and VPE are shown in Fig. 12(a) and those corresponding to path loss models are shown in Fig. 12(b). The  $x$ -axis is the distance along the tunnel, where the locations of the APs are marked. The  $y$ -axis is the index of the associated AP. Fig. 13 shows the ray tracing, VPE, and measured RSS experienced by a train moving along the entire track. This *train* RSS is obtained after processing the raw RSS shown in Fig. 7 according to the RSS-based handoff algorithm presented in the previous subsection. Therefore, the deviations observed in Fig. 13 result from differences in the location where the train changes its association. Table V lists the handoff locations along with the associated APs corresponding to Figs. 12(a) and 12(b). It can be seen that both ray tracing and VPE, produce the same number of handoffs as the measurements and also to the same APs. However, the path loss models either underpredict (in [25], [26]) or overpredict (in [27]) the number of handoffs. This is primarily due to the fact that the rich multipath in such complex tunnel environments is not adequately captured by the path loss models, especially around the decision point, where the signal drops below  $P_{th}$  and a handoff is most likely to be initiated. Moreover, it should be noted from the first row of Table V that the train never made an association with AP-5 based on the measured values of RSS. This redundancy, which cannot be found unless the handoff algorithm is defined and studied, illustrates the limitations of the current fragmented approach to network planning and the potential for efficiency gains carried by an integrated approach.

## VI. CONCLUSION

This paper demonstrated the use of physics-based propagation modeling techniques as a preplanning network design tool for train communication systems. The proposed integration of ray tracing and parabolic equation solvers with network-level performance evaluation methods culminated in a comprehensive, physics-driven approach to the analysis and design of

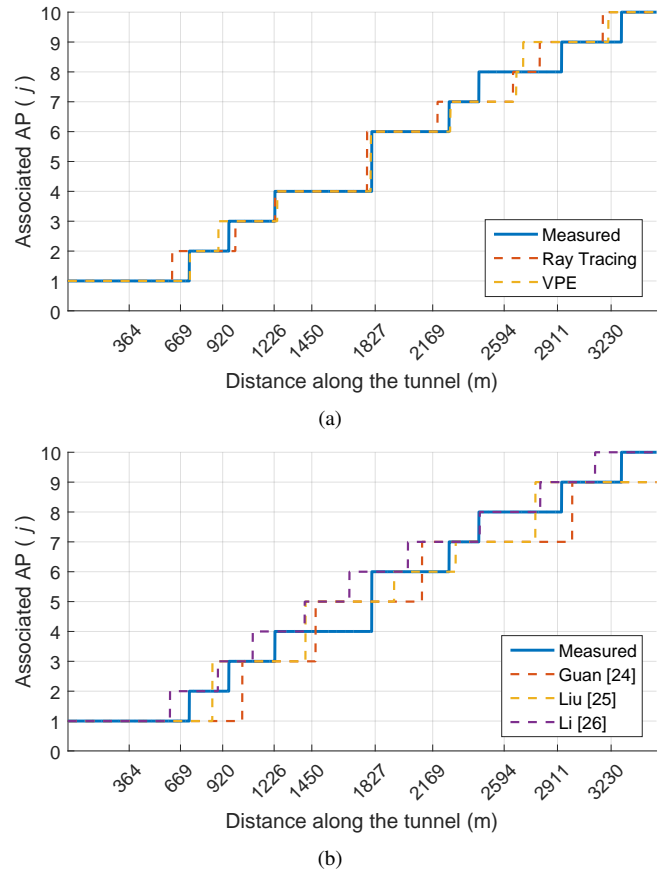


Fig. 12. Handoff map for measurements compared with that of (a) simulated models, and (b) path loss models.

a train communication system. The same approach can be readily extended to other communication systems and sensor networks.

Based on the results of this work, new applications of physics-based propagation models can be envisioned. For example, the joint optimization of access point placement and network protocols can be performed, as opposed to separately pursuing these two tasks. To this end, this paper presented the example of a handoff map calculation in a complex and rather rugged environment such as that of the London Underground. We demonstrated that a mean error level in the 4–6 dB range in the path loss estimation by ray tracing or VPE was sufficient to reproduce a handoff map that closely approximated the one

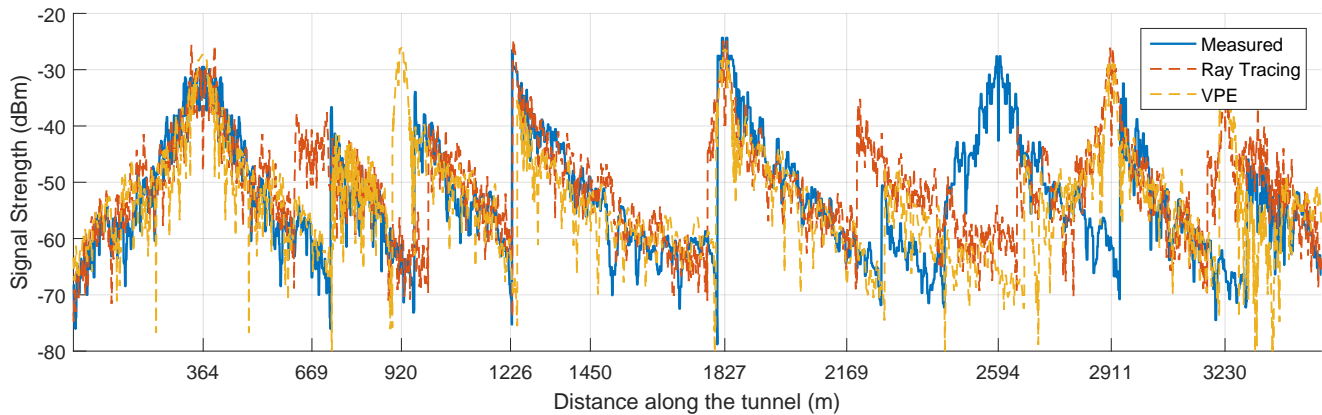


Fig. 13. Comparison of signal strength (dBm) along the tunnel as received by the train.

produced using measured RSS values. This first, yet necessary step paves the way for the full integration of propagation models with network simulators and the co-design of the infrastructure of a network and its network algorithms, fully harnessing the physics of radio wave propagation to enhance their robustness.

#### REFERENCES

- [1] J. Farooq and J. Soler, "Radio communication for communications-based train control (cbtc): A tutorial and survey," *IEEE Commun. Surveys & Tuts.*, vol. 19, no. 3, pp. 1377–1402, Jan. 2017.
- [2] S. Morar, "Evolution of communication based train control worldwide," *IET Conference Proceedings*, pp. 281–289(8), Jan. 2010.
- [3] R. D. Pascoe and T. N. Eichorn, "What is communication-based train control?" *IEEE Veh. Technol. Mag.*, vol. 4, no. 4, pp. 16–21, Dec. 2009.
- [4] T. K. Sarkar, Z. Ji, K. Kim, A. Medouri, and M. Salazar-Palma, "A survey of various propagation models for mobile communication," *IEEE Antennas Propag. Mag.*, vol. 45, no. 3, pp. 51–82, Jun. 2003.
- [5] J. R. Wait, "Theory of EM wave propagation through tunnels," *Radio Science*, vol. 10, no. 7, pp. 753–759, 1975.
- [6] K. D. Laakmann and W. H. Steier, "Waveguides: characteristic modes of hollow rectangular dielectric waveguides," *Applied optics*, vol. 15, no. 5, pp. 1334–40, May 1976.
- [7] L. Deryck, "Natural propagation of electromagnetic waves in tunnels," *IEEE Trans. Veh. Technol.*, vol. 27, no. 3, pp. 145–150, Aug. 1978.
- [8] S. F. Mahmoud, "Modal propagation of high frequency electromagnetic waves in straight and curved tunnels within the earth," *Journal of Electromagnetic Waves and Applications*, vol. 19, no. 12, pp. 1611–1627, 2005.
- [9] D. G. Dudley, M. Lienard, S. F. Mahmoud, and P. Degauque, "Wireless propagation in tunnels," *IEEE Antennas Propag. Mag.*, vol. 49, no. 2, pp. 11–26, Apr. 2007.
- [10] X. Zhang and C. D. Sarris, "Vector parabolic equation-based derivation of rectangular waveguide surrogate models of arched tunnels," *IEEE Trans. Antennas Propag.*, vol. 66, no. 3, pp. 1392–1403, Mar. 2018.
- [11] A. V. Popov, V. A. Vinogradov, N. Y. Zhu, and F. M. Landstorfer, "3D parabolic equation model of EM wave propagation in tunnels," *Electron. Lett.*, vol. 35, no. 11, pp. 880–882, May 1999.
- [12] R. Martelly and R. Janaswamy, "An ADI-PE approach for modeling radio transmission loss in tunnels," *IEEE Trans. Antennas Propag.*, vol. 57, no. 6, pp. 1759–1770, Jun. 2009.
- [13] P. Bernardi, D. Caratelli, R. Cicchetti, V. Schena, and O. Testa, "A numerical scheme for the solution of the vector parabolic equation governing the radio wave propagation in straight and curved rectangular tunnels," *IEEE Trans. Antennas Propag.*, vol. 57, no. 10, pp. 3249–3257, Oct. 2009.
- [14] X. Zhang and C. D. Sarris, "A high-accuracy ADI scheme for the vector parabolic equation applied to the modeling of wave propagation in tunnels," *IEEE Antennas and Wireless Propag. Lett.*, vol. 13, pp. 650–653, 2014.
- [15] X. Zhang, N. Sood, J. K. Siu, and C. D. Sarris, "A hybrid ray-tracing/vector parabolic equation method for propagation modeling in train communication channels," *IEEE Trans. Antennas Propag.*, vol. 64, no. 5, pp. 1840–1849, May 2016.
- [16] X. Zhang and C. D. Sarris, "A Gaussian beam approximation approach for embedding antennas into vector parabolic equation based wireless channel propagation models," *IEEE Trans. Antennas Propag.*, vol. 65, no. 2, pp. 1840–1849, Feb. 2017.
- [17] S.-H. Chen and S.-K. Jeng, "SBR image approach for radio wave propagation in tunnels with and without traffic," *IEEE Trans. Veh. Technol.*, vol. 45, no. 3, pp. 570–578, Aug. 1996.
- [18] D. Didascalou, T. M. Schafer, F. Weinmann, and W. Wiesbeck, "Ray-density normalization for ray-optical wave propagation modeling in arbitrarily shaped tunnels," *IEEE Trans. Antennas Propag.*, vol. 48, no. 9, pp. 1316–1325, Sep. 2000.
- [19] E. Masson, P. Combeau, M. Berbineau, R. Vauzelle, and Y. Poussel, "Radio wave propagation in arched cross section tunnels - simulations and measurements," *Journal of Communication*, vol. 4, no. 4, pp. 276–283, May 2009.
- [20] K. Guan, Z. Zhong, J. I. Alonso, and C. Briso-Rodríguez, "Measurement of distributed antenna systems at 2.4 GHz in a realistic subway tunnel environment," *IEEE Trans. Veh. Technol.*, vol. 61, no. 2, pp. 834–837, Dec. 2012.
- [21] J.-M. Molina-Garcia-Pardo, M. Lienard, and P. Degauque, "Propagation in tunnels: Experimental investigations and channel modeling in a wide frequency band for MIMO applications," *EURASIP Journal on Wireless Communications and Networking*, vol. 2009, no. 1, pp. 560–571, 2009.
- [22] X. Cai, X. Yin, X. Cheng, and A. P. Yuste, "An empirical random-cluster model for subway channels based on passive measurements in UMTS," *IEEE Trans. Commun.*, vol. 64, no. 8, pp. 3563–3575, Jun. 2016.
- [23] Y.-P. Zhang, Z. Jiang, T.-S. Ng, and J. Sheng, "Measurements of the propagation of UHF radio waves on an underground railway train," *IEEE Trans. Veh. Technol.*, vol. 49, no. 4, pp. 1342–1347, Jul. 2000.
- [24] M.-S. Choi, D.-Y. Kim, H.-S. Jo, J.-G. Yook, and H.-K. Park, "Path-loss characteristics in subway tunnels at 2.65 GHz," *Microwave and Optical Technology Letters*, vol. 48, no. 2, pp. 383–386, 2006.
- [25] K. Guan, B. Ai, Z. Zhong, C. F. López, L. Zhang, C. Briso-Rodríguez, A. Hrovat, B. Zhang, R. He, and T. Tang, "Measurements and analysis of large-scale fading characteristics in curved subway tunnels at 920 MHz, 2400 MHz, and 5705 MHz," *IEEE Trans. Intell. Transp. Syst.*, vol. 16, no. 5, pp. 2393–2405, Mar. 2015.
- [26] R. Liu, I. J. Wassell, and K. Soga, "Relay node placement for wireless sensor networks deployed in tunnels," in *In Proc. IEEE Conference on Wireless and Mobile Computing, Networking and Communications*, Oct. 2010, pp. 144–150.
- [27] L. Jinxing, Z. Youping, Z. Jing, J. Rui, T. Cheng, and T. Zhenhui, "Radio channel measurements and analysis at 2.4/5GHz in subway tunnels," *China Communications*, vol. 12, no. 1, pp. 36–45, Apr. 2015.
- [28] M. Y. Chan, S. Baroudi, J. Siu, and J. Liebeherr, "Measurement-based handover method for communication-based train control systems," in *Proc. IEEE 86th Vehicular Technology Conference (VTC-Fall)*, Sept 2017.

- [29] T. S. Rappaport *et al.*, *Wireless communications: principles and practice*. vol. 2, Prentice Hall, New Jersey, 1996.
- [30] N. Sood, L. Liang, S. V. Hum, and C. D. Sarris, "Ray-tracing based modeling of ultra-wideband pulse propagation in railway tunnels," in *IEEE International Symposium on Antennas and Propagation (APSURSI)*, July 2011, pp. 2383–2386.
- [31] N. Sood and C. D. Sarris, "Enabling accurate propagation modeling of complex tunnel geometries with ray-tracing," in *IEEE International Symposium on Antennas and Propagation USNC/URSI National Radio Science Meeting*, July 2017, pp. 1827–1828.
- [32] M. F. Cátedra and J. Perez, *Cell planning for wireless communications*. Artech House, Inc., 1999.
- [33] D. L. Sengupta and V. V. Liepa, *Applied Electromagnetics and Electromagnetic Compatibility*. Wiley, 2005.
- [34] M. Levy, *Parabolic equation methods for electromagnetic wave propagation*. London, U.K.: Inst. Elect. Eng., 2000.
- [35] X. Zhang and C. D. Sarris, "Error analysis and comparative study of numerical methods for the parabolic equation applied to tunnel propagation modeling," *IEEE Trans. Antennas Propag.*, vol. 63, no. 7, pp. 3025–3034, Jul. 2015.
- [36] E. Masson, P. Combeau, Y. Cocheril, M. Berbineau, L. Aveneau, and R. Vauzelle, "Radio wave propagation in arch-shaped tunnels: Measurements and simulations by asymptotic methods," *Comptes Rendus Physique*, vol. 11, no. 1, pp. 44 – 53, 2010, propagation and remote sensing.
- [37] Y. Zhang, Y. Hwang, and R. Kouyoumjian, "Ray-optical prediction of radio-wave propagation characteristics in tunnel environments. 2. Analysis and measurements," *IEEE Trans. Antennas Propag.*, vol. 46, no. 9, pp. 1337–1345, 1998.
- [38] C. J. Willmott and K. Matsuura, "Advantages of the mean absolute error (MAE) over the root mean square error (RMSE) in assessing average model performance," *Climate Research*, vol. 30, no. 1, pp. 79–82, 2005.
- [39] A. Austin, N. Sood, J. Siu, and C. D. Sarris, "Application of polynomial chaos to quantify uncertainty in deterministic channel models," *Antennas and Propagation, IEEE Transactions on*, vol. PP, no. 99, pp. 1–1, 2013.
- [40] B. Sklar, *Digital communications*. vol. 2, Prentice Hall Upper Saddle River, 2001.
- [41] G. P. Pollini, "Trends in handover design," *IEEE Commun. Mag.*, vol. 34, no. 3, pp. 82–90, Mar. 1996.
- [42] Cisco Systems Inc, "RF power values," <http://www.cisco.com/c/en/us/support/docs/wireless-mobility/wireless-lan-wlan/23231-powervalues-23231.html>, 2008.